Journal of the Iranian Chemical Society
https://doi.org/10.1007/s13738-023-02874-y

ORIGINAL PAPER

Removal of heavy metals by using magnetically reusable Fe_3O_4@ZnO nanocomposites from *Andrographis paniculata* leaf extract: a greener way to remove industrial effluents

M. S. Manojkumar[1] · S. Mohan[2] · C. Thangamani[3] · V. Shanmugam[4]

Received: 9 November 2022 / Accepted: 9 August 2023
© Iranian Chemical Society 2023

Abstract
The ability to repurpose adsorbent was critical for making the sewage treatment system both premium and environmentally beneficial. Toxic metals ions [Pb(II), Cr(II), and Cd(II)] were removed from effluent discharge using Fe_3O_4/ZnO nanoparticles as sorbent materials. Chemical affinity, zero potentials, XRD, FTIR, and TEM were used to explore the structural and interfaces adsorption process of Fe_3O_4/ZnO composite in this study. Experiments on absorption, desorption, and recycling were performed. The findings demonstrate that perhaps the toxic metals substituted for H in the Fe–O–H structure and formed the Zn–O–Me structure, implying that metal elimination was accomplished through ion exchange. Cd(II), Pb(II), and Cr(IV) had 99.81%, 99.76%, 98.1%, respectively,adsorptive degradation efficiency. The Langmuir model was shown to be the best fit for describing the absorption on the surface of Fe_3O_4/ZnO nanoparticles based on the stability data processing. The kinetic parameters of toxic metal ions on the surface of Fe_3O_4/ZnO composites were relatively similar to the pseudo-second-order concept, according to the kinetics investigations. The trials proved that reprocessing the Fe_3O_4/ZnO sorbent extracted from water by a magnetic material was a viable option for removing pollutants in an environmentally acceptable and effective manner.

Keywords Heavy metals · Fe_3O_4/ZnO · Adsorption · Magnetite · Langmuir isotherm

Introduction

Presently, ecological regulation is a serious problem in the world. Water contamination is probably one of the most concerning aspects of society. A large variety of emissions, such as toxic metals, colors, and fertilizers, reach various waterways and become important contributors of groundwater contamination. Toxic metals are particularly dangerous because of their great water fluidity and greater accessibility to live bodies across the food system, resulting in a variety of health complications [1–7]. Lead (Pb), chromium (Cr), and cadmium (Cd) are one of the toxic substances that are a major contaminant and are extensively distributed [3]. Consuming contaminated watercourses via a range of sources, including electrolysis, mine, metal polishing, and lead, chromium, and cadmium casting [8]. Various approaches for removing contaminants have been intensively examined in the literature. To eliminate toxic metal ions from polluted water, various methods such as co-precipitation, electrochemical methods, membrane processes, and absorption have been developed.

✉ M. S. Manojkumar
msmanojkumar1987@gmail.com

✉ S. Mohan
mohans@vicas.org

[1] Department of Biotechnology, Vivekanadha College of Engineering for Women, Elayampalam, Namakkal 637210, Tamilnadu, India

[2] Department of Chemistry, Vivekanandha College of Arts and Science for Women (Autonomous), Elayampalayam, Namakkal 637209, Tamilnadu, India

[3] Department of Physics, M. Kumarasamy College of Engineering (Affiliated to Anna University, Chennai), Karur 639006, Tamilnadu, India

[4] Department of Physics, Government Arts College (Autonomous), Karur-5 (Affiliated to Bharathidasan University), Tiruchirappalli, Tamilnadu, India

Published online: 09 September 2023

Because of its high removal effectiveness, dependability, affordability, and lack of toxic by-products, adsorption was an appealing strategy in polluted water remediation among these approaches. Several methods for developing less expensive and more powerful material adsorbents have previously been explored. Minerals have received more attention in the last decade for toxic substances cleanup treatments due to their excellent sorption capacities [8, 9]. The nano-structured material, in particular, offers extremely large surface areas, resulting in high capacity and the ability to improve contaminants adhesion with the interface [10, 11]. As a result, Fe_3O_4/ZnO was chosen as a component in the preparation of overlayed sorbent materials for the elimination of heavy metals [12, 13]. Regrettably, such materials still had difficulty with removal from polluted water, as they preferred to form ultrafine granules in aqueous phase, resulting in prior to actual. As a result, the creation of novel nano-sorbents with easy separation properties and reuse potential has piqued our attention. Due to their strong magnetic permeability, iron oxides like magnetite (Fe_3O_4) and magnetite (υ-Fe_2O_3) have been widely used in construction. The addition of Fe_3O_4/ZnO in the aqueous solution resulted in excellent removal of heavy metals, and also retained its magnetic properties. Interface functionalization was discovered to be responsible for the absorption. There was a limitation of understanding of exterior structure-sensitive absorption and the operation of absorption. It is still unclear how the variable impact on heavy metals adhesion and the adsorbent's effectiveness multiple periods reuse.

The esters of hydroxybenzoic acid, generally known as parabens, were used in a wide range of industries. They have excellent antimicrobial ability, and were extensively used in cosmetics, food, and pharmaceutical industries. Despite its uses, parabens can cause endocrine disruption functions, increase the risk of breast cancer, and other side effects. SPME synthesized in submicro-sizes by molecular imprinted polymers are used to identify parabens in water samples. The SPME can identify benzyl, methyl, and propyl parabens in water samples [35]. Corona charged aerosol detectors were used in the detection of parabens in cosmetic products. Carbon nanotubes are used to remove parabens in solid phase extraction [36]. As research in parabens was considered, sorbents are primarily used in detection rather than removal.

There is various nanomaterials that have been used in the removal of heavy metals; however, the complete adsorption of heavy metals from the industrial effluents is a difficult process. The usage of Fe_3O_4/ZnO in this study has helped in maximum removal of heavy metals.

The study aims on eliminating heavy metals from industrial effluents using Fe_3O_4/ZnO composites as cycling sorbents. Structural, optical properties and Fe_3O_4/ZnO composites performance were investigated. Permeate parameters were evaluated to eliminate wastewater pollutants. Toxic metals such as Pb (II), Cr (IV), and Cd (II) were removed from industrial effluents using Fe_3O_4/ZnO composites as cycling sorbents. The composite materials' molecular affinity and cumulative capability were considered to be effective against certain heavy metals in wastewater. Fe_3O_4/ZnO composites' surface adsorption behavior and kinetics were examined. Heavy metal adsorption and desorption, as well as recycling, were investigated. The metal uptake methods of Fe_3O_4/ZnO nanocomposite sorbent have been explored.

Throughout this content analysis, core–shell Fe_3O_4/ZnO nanoparticles have been synthesized and used to accumulate commercial effluents such as lead, chromium, and cadmium ions. The influence of interaction period, aqueous phase pH, catalyst dosage, initial effluent composition, and heating rate on adsorption was evaluated. Following that, the kinetic models, stability, and heat transfer analyses have been examined.

Experimental

All the chemicals and reagents are obtained from sigma Aldrich chemicals Pvt. Ltd. Metal precursors are such as Zn $(OAC)_2$ 99.8% $FeCl_2.4H_2O > 99.8\%$ and $FeCl_3.5H_2O > 99.9\%$, $NH_4OH > 99.9\%$, respectively. The following chemicals and reagents are used as a without further purification. The commercial effluents were prepared in our laboratory. The commercial effluents such as cadmium nitrate, lead phosphate, and potassium dichromate are observed.

Healthy and potential leaves of *Andrographis paniculata* were originated from local area in Karur, Tamilnadu, India. The obtained leaves were washed with several times deionized water and dried for about an hour's. Later the collected powder for further treatment is used.

Greener synthesis of Fe_3O_4 nanoparticles

At 80 °C, 10 g of crisped *Andrographis paniculata leaf extract* was injected into demineralized water. The leaf extract of *Andrographis paniculata* has been used because when they come into contact, the nanoparticles can be produced rapidly and reduce the time consumption. The water extract was used to make Fe_3O_4 MCNPs after the combination had been diffused for 2 h. $FeCl_3$ (2 mmol) and $FeCl_2$ (1 mmol) were added to a 100-mL *Andrographis paniculata leaf* water extract in a two-necked round-bottomed flask (250 mL). Under an inert atmosphere and at room temperature, a solution of NH_4OH (9 M, 10 mL) was gently added to the mixture. External magnetic field was used to develop and detach the pure black crude product from the precursor solution, which was then vacuumed with washed repeatedly before being oxidized in an oven at 80^0C for 24 h [14].

Design and fabrication of Fe_3O_4/ZnO nanocomposites

The design and build of Fe_3O_4/ZnO NCs in demineralized water, 1.5 g of Zn $(OAC)_2$ and 1.5 g of $FeCl_2.4H_2O$ and 1.5 g of $FeCl_3.5H_2O$ were solubilized (10 mL). In a round-bottomed flask at 85 °C for 8 h, *Andrographis paniculata leaf* (APL) extract (30 mL) was gradually added to the reaction mixture. To eliminate undesirable plant-based matter, the mixture was cooled to room temperature, sonicated for 10 min, resuspended at 7000 rpm for around 10 min, and afterward purified. Pre-filter was used to accumulate the crude product, which was then scrubbed multiple rinsed with deionized water and ethanol (96%). The specimens were then warmed for 1 h at 50 °C. The fabrication of Fe_3O_4/ZnO NCs was dehydrated in the air for 24 h at room temperature [15]. The extracted nanocomposite was stable in condition. According to the UV results, the adsorption of nanocomposite is at a higher peach value compared to ferrous oxide. The interaction between the composites plays an important role in adsorption of effluents.

Heavy metals removal investigation

Heavy metals (Pb (II), Cd (II), Cr (IV)) were present in commercial effluent at concentrations of 10 mg L^1. To consider removing toxic metals from industrial effluents, a magnetic Fe_3O_4/ZnO composite was used as an adsorption process. The adsorptive Fe_3O_4/ZnO composites were implanted in contaminated water and agitated for 24 h on a spinning tank (20 rpm). The heavy metal removal investigations were performed at pH levels ranging from 2 to 12 and temperatures tend to range from 30 to 60 °C. The adsorptive composites were then gathered from the solution using an NdFeB magnet. After removing the toxic substances, the contaminated water was analyzed using inductively coupled plasma emission spectra spectrophotometer (ICP). Every batch process was repeated three times, as well as the comparable discrepancy was noticed to be less than 2%, with the final results being the sample mean. The expulsion level was predicted using the capacity of retrieval of heavy metal ions in solution prior to actually and during the adsorption, and the expressions be as follows

$$q_e = C_0 - C_e/C_0 \tag{1}$$

where q_e (%) was the removal degree, C_0 and C_e (mg L^{-1}) were the initial and final metals concentrations in the solution, respectively.

For the adsorptive investigation, Fe_3O_4/ZnO packing toxic metals were immersed into the 0.1 M HCl solution, and the resulting mixture was shaken vigorously in a shaking incubator at 30 °C for 0.5 h. The composite feedstock was then gathered using a NdFeB magnet, and metal ion doses in the solution were measured. Upon rinsing, Fe_3O_4/ZnO nanocomposite have been used in the succeeding adsorbent cycle. The amount of ions desorption per unit volume of adsorptive used was calculated from the respective approximation

$$q_{de} = CV_0/m_0 \times 100 \tag{2}$$

whereas q_{de} (percent) was the desorption degree (percent), C was the metal ion accumulations in the desorption solution (mg L^1), V_0 was the volume of the desorption solution (L), and m_0 was the quantity of toxic metal ions in before desorption (mg).

Adsorption isotherm

The Freundlich and Langmuir ideas have already been employed to investigate adsorption characteristics [16, 17]. The Langmuir isotherm model was determined by calculating the adsorption performance and offered the adsorbent's fairly homogeneous acceleration. This isotherm also implied monolayer adsorption. Equation denotes the simple regression analysis of the Langmuir Eq. (3). The Freundlich arithmetic described both monolayer and multilayer adsorbents. Freundlich isotherm models were traditionally used to identify strong adsorption ability. Equation affirms the linear function of the Freundlich model (4)

$$\text{Langmuir adsorption isotherm;}\ \ C_e/q_e = 1/kq_m + C_e/q_m \tag{3}$$

$$\text{Freundlich isotherm;}\ \ \log q_e = \log k' + 1/n\ \log\ C_e \tag{4}$$

where the C_e and q_e were the equilibrium concentration of heavy metal ions (mol L^{-1}) and the amount of heavy metal ions adsorption on the mineral at equilibrium (mg g^{-1}), respectively. k was the Langmuir isotherm constant, and q_m was the maximum monolayer coverage capacities (mg g^{-1}), n was related to adsorption capacity and k' was the Freundlich isotherm constant (mg g^{-1}) (L mg^{-1}) (Tables 1, 2, 3).

Adsorption kinetics

Study of the adsorption kinetics provided the rate of adsorbed heavy metal ions on the surface of sorbent pseudo-first- and pseudo-second order models that were the most common kinetic models used for modeling the kinetic rates [18] These models were also estimated the amount of adsorbed heavy metals on the surface of sorbent at various time intervals.

Table 1 Different parameters of various isotherm models of Fe_3O_4/ZnO nanoparticles

Heavy metals	Langmuir isotherm			Freundich isotherm		
	q_m (mg g^{-1})	K	R^2	K'	n	R^2
Cd^{2+}	568.3	7.92	0.9920	152.3	2.673	0.798
Cr^{4+}	602.6	0.90	0.978	160.9	2.920	0.934
Pb^{2+}	670.2	3.26	0.992	178.26	2.82	0.936

Table 2 Kinetic adsorption parameter of Fe_3O_4/ZnO nanoparticles

Heavy metals	Pseudo-first order		Pseudo-second order	
	K_L	R^2	K	R^2
Cd^{2+}	0.0042	0.9599	0.0386	0.998
Cr^{4+}	0.0038	0.9402	0.0142	0.999
Pb^{2+}	0.0061	0.7382	0.0048	0.994

The equations of these models can be expressed as follows. The pseudo-first-order kinetic equation was represented by Eq. (5).

$$\ln\left(q_e - q_t\right) = \ln q_e - k_L t \tag{5}$$

The pseudo-second-order (PSO) kinetic equation was represented by Eq. (6).

$$t/q_t = 1/kq_e^2 + 1/q_e \times t \tag{6}$$

where q_e and q_t were the heavy ions adsorption quantity (mg g^{-1}) at equilibrium time and time t, respectively, k_L and k were the rate constants of pseudo-first and second order models, respectively. Q_t had exponential relation with t in the pseudo-first-order model while the relation between t/q_t and t was linear for the pseudo-second-order model (Fig. 1).

Results and discussion

UV absorption spectra analysis

Figure 2 illustrates the UV–visible recognizable peaks of Fe_3O_4 and Fe_3O_4/ZnO NCs. Because once AP leaf extract was infused with $Zn(OAC)_2$ and $FeCl_2{\cdot}4H_2O$ and $FeCl_3{\cdot}5H_2O$, the color was observed from white to brown, which was credited to the formation of Fe_3O_4/ZnO NCs. However, insignificant absorption at 300–400 nm is observed, which might be attributed to the spin-flip transition of the Fe–Fe pair. The color variations are accompanied by the fluctuation of localized surface plasmonic resonance of Fe_3O_4/ZnO nanocomposites (LSR). The broad absorption peaks were found to be near 319 nm, indicating a substantial decrease of Zn $(OAC)_2$ and Fe^{3+}/Fe^{2+} into Fe_3O_4/ZnO

Table 3 Thermodynamic parameters for adsorption of Fe_3O_4/ZnO nanoparticles on Cd^{2+}, Cr^{4+}, Pb^{2+}

Heavy metals	ΔH^0 (J mol^{-1})	ΔS^0 (J mol^{-1} K^{-1})	ΔG^0			
			298^0	303^0	313^0	323^0
Cd^{2+}	− 18.936	− 49.274	− 4.793	− 4.632	− 4.321	− 3.261
Cr^{4+}	− 20.638	− 54.283	− 6.234	− 6.123	− 6.012	− 5.234
Pb^{2+}	− 24.726	− 58.324	− 7.322	− 7.221	− 7.023	− 6.023

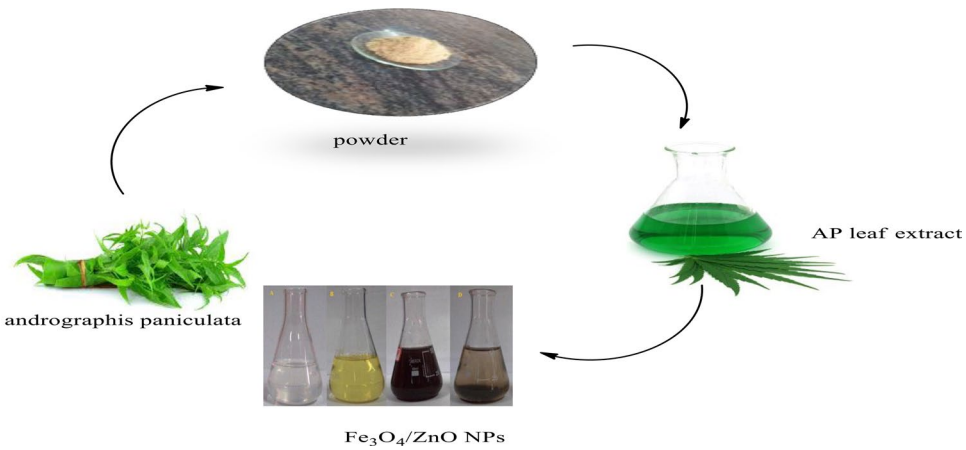


Fig. 1 Scheme; formation of Fe_3O_4@ZnO nanoparticles using green synthesis route

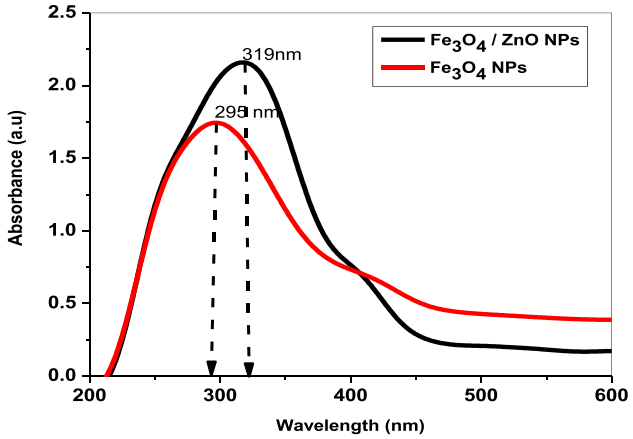


Fig. 2 UV Absorption spectra of **a** green synthesized Fe_3O_4 NPs, **b** Fe_3O_4@ZnO NPs by green approach

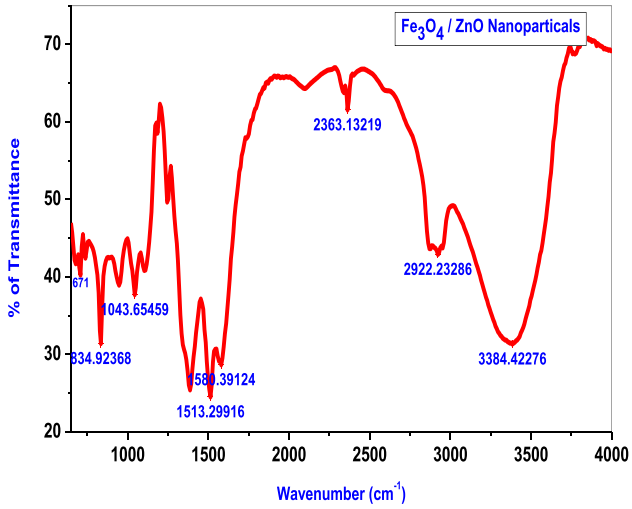


Fig. 3 Representation of functional group analysis of Fe_3O_4@ZnO nanoparticles using APL extract

nanocomposites. In a study, the adsorption peaks have been observed at 295–319 nm. The shift of the absorption band of the samples shows an alteration in the electronic move and bandgap. The quantum confinement effect led the shoulder band to shift toward a higher wavelength (red-shifted).

Fourier transforms infrared spectroscopy (FTIR) analysis

Figure 3 depicts the FTIR spectrum of eco-friendly synthesized Fe_3O_4/ZnO NCs. The frequency spectrum bands at 3384.4 cm^{-1} have been caused by O–H stretching. The band around 2363–2922 cm^{-1} is engendered by C–H stretching vibrations. C=O stretching was induced above a peak range of 1650 cm^{-1}. The peaks at 1043 cm^{-1} coincide to Fe–O–Zn twisting compressive motions. The squeezing variants for the emergence of Fe_3O_4/ZnO nanoparticles are delegated to the potent excitations frequency band at 671 cm^{-1}. As a consequence of the FTIR survey, Fe_3O_4/ZnO NCs are preserved from becoming ascertained by the bioactive constituents of *Andrographis paniculata* leaf by stabilizing the exterior of nanocomposites during synthesis process [19–21].

X-ray diffraction analysis

XRD was used to investigate the phase and structural components of Fe_3O_4/ZnO nanocomposites in (Fig. 4). The cubic spinel magnetite component is visible in the XRD analysis of Fe_3O_4, with crystallography peaks at 30.20°, 35.59°, 43.22°, 54.04°, 57.25°, and 62.87°, corresponding to the (220), (311), (400), (422), (511), and (440) planes, respectively. The XRD behavior of Fe_3O_4/ZnO NCs shows all magnetite defining feature peaks as well as crystallography peaks at 31.76°, 34.42°, 36.08°, 47.53°, 56.76°, and 62.80° that can be accessed to (100), (002), (101), (102), (110), and (112) planes of the hexagonal wurtzite phase of ZnO. This indicates that the ZnO shell was successfully formed without any phase transition of the Fe_3O_4 nanoparticles [22].

SEM/EDX analysis

SEM investigation was used to examine the architecture of Fe_3O_4/ZnO nanoparticles. The outcome of the study shows that the fabricated Fe_3O_4/ZnO particles were globular and consolidated into an anisotropic material with a mean size of 18 nm, as shown in Fig. 4a–c. The powder particles were found to be somewhat clustered [23]. Figure 4d shows the energy-dispersive X-ray spectrum of the green fabricated Fe_3O_4/ZnO nanoparticles specimens, which confirms the existence of Fe, Zn, and O constituents. The absence of an imperfection band in the EDX spectrum proves that the synthesized samples are genuine and also demonstrates the homogenous allocation of the individual components.

TEM/HRTEM analysis

The TEM appearance and SAED profile of Fe_3O_4/ZnO NCs developed using the greener approaches are shown in Fig. 5a, b. The mean particle size in Fig. 5a was determined to be 11 nm, which was quite close to the crystalline phase predicted in the XRD pattern using Debye Scherrer's model. Figure 5b shows that the reflection bands in the SAED illustration correspond the XRD profile, confirming the crystallite size and anatase phase of Fe_3O_4/ZnO nanoparticles [24].

The DLS method was used to identify the particle sizes and average diameter of the synthesized Fe_3O_4/ZnO, as seen in Fig. 5d. Following figure states that the overall size and monodispersity index (PdI) of the synthesis Fe_3O_4/ZnO

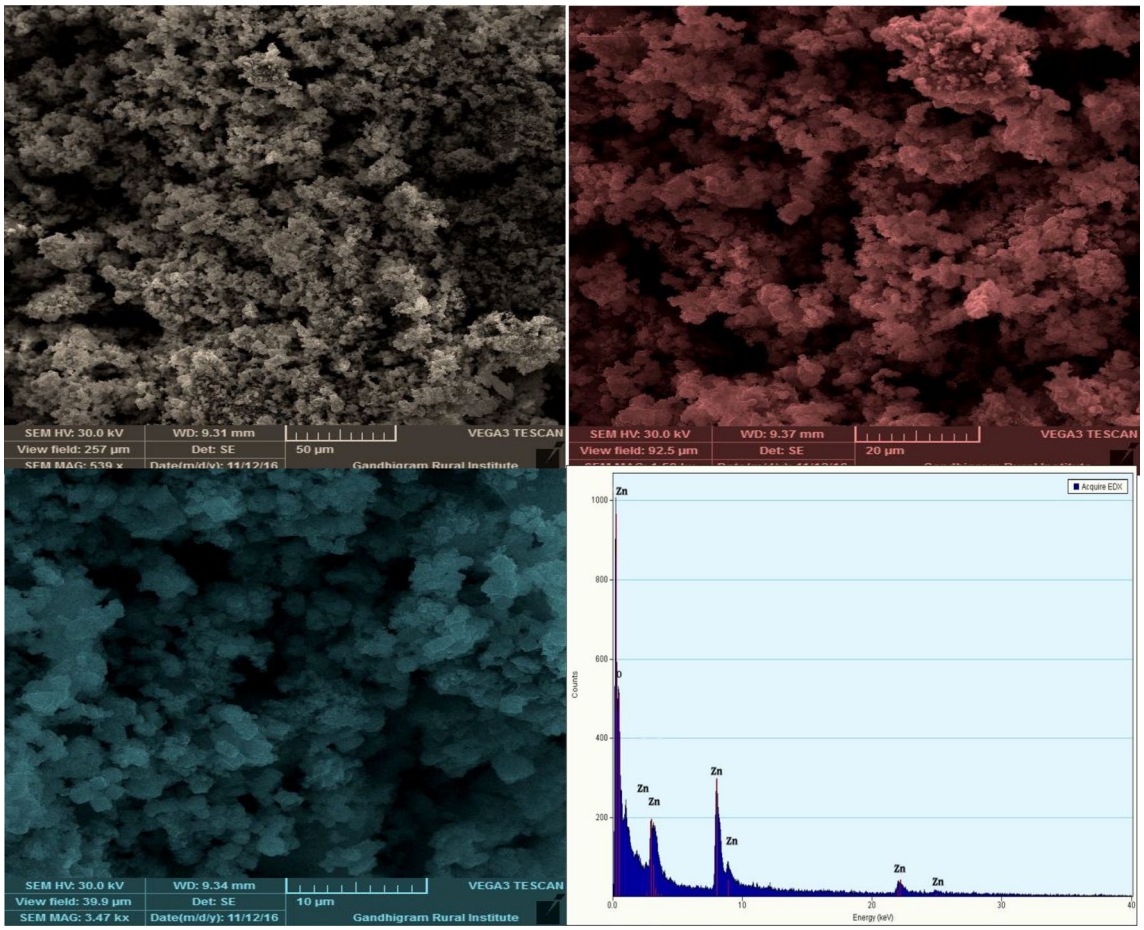


Fig. 4 SEM profile of Fe_3O_4@ZnO nanoparticles via green approach using APL extract

using APL extract and derivatives were 295 and 0.31 nm, respectively, and 61.44 and 0.42 nm. The calibrated z-average and polydispersity index of the synthesized Fe_3O_4/ZnO NCs show that they are narrow size distribution, correlating with the facts provided either by distributor and ultraviolet–visible [25].

Zeta potential analysis

As measured by zeta potential analyzer, Fe_3O_4/ZnO particles were negatively charged with value of − 32.6 mV as shown in Fig. 6. The negatively charged surface of Fe_3O_4/ZnO particles was mainly contributed by the OH^- groups during the growth process as discussed by Thein et al. [26] These OH^- groups became the actively adsorptive sites. As depicted in Fig. 6, the cationic of heavy metal in the aqueous solution tended to react with OH^- groups to form a thin film on the surface of Fe_3O_4/ZnO particles. Similar observation was also reported by Wang et al. [27]. As the adsorption process was limited by the number of negative adsorptive sites on the surface of Fe_3O_4/ZnO particles, the adsorption efficiency was usually poor and might reach a saturation level after a period of time. As the optical energy of visible light was insufficient to cause Fe_3O_4/ZnO particles generate electrons and holes, thus the removal of metal ions from solution by Fe_3O_4/ZnO particles was via physical adsorption process.

BET isotherm spectra

The Brunauer–Emmett–Teller (BET) surface area analysis tool was used to determine the actual area of produced nanomaterials. Barrett–Joyner–Halenda study also yielded other results, such as pore diameter and average pore are shown in Fig. 7c. The produced Fe_3O_4/ZnO NPs exhibited an excellent surface area of 105 $m^2\ g^{-1}$, a pore size of 10.50 nm, and a volume fraction of 0.278 cm^3/g, which will be useful for adsorption in the treatment of infected (Pb(II), Cr(IV), and Cd (II)) wastewater. Figure 7b shows the acquired adsorption–desorption isotherm models shape of the produced Fe_3O_4/ZnO nanoparticles [28].

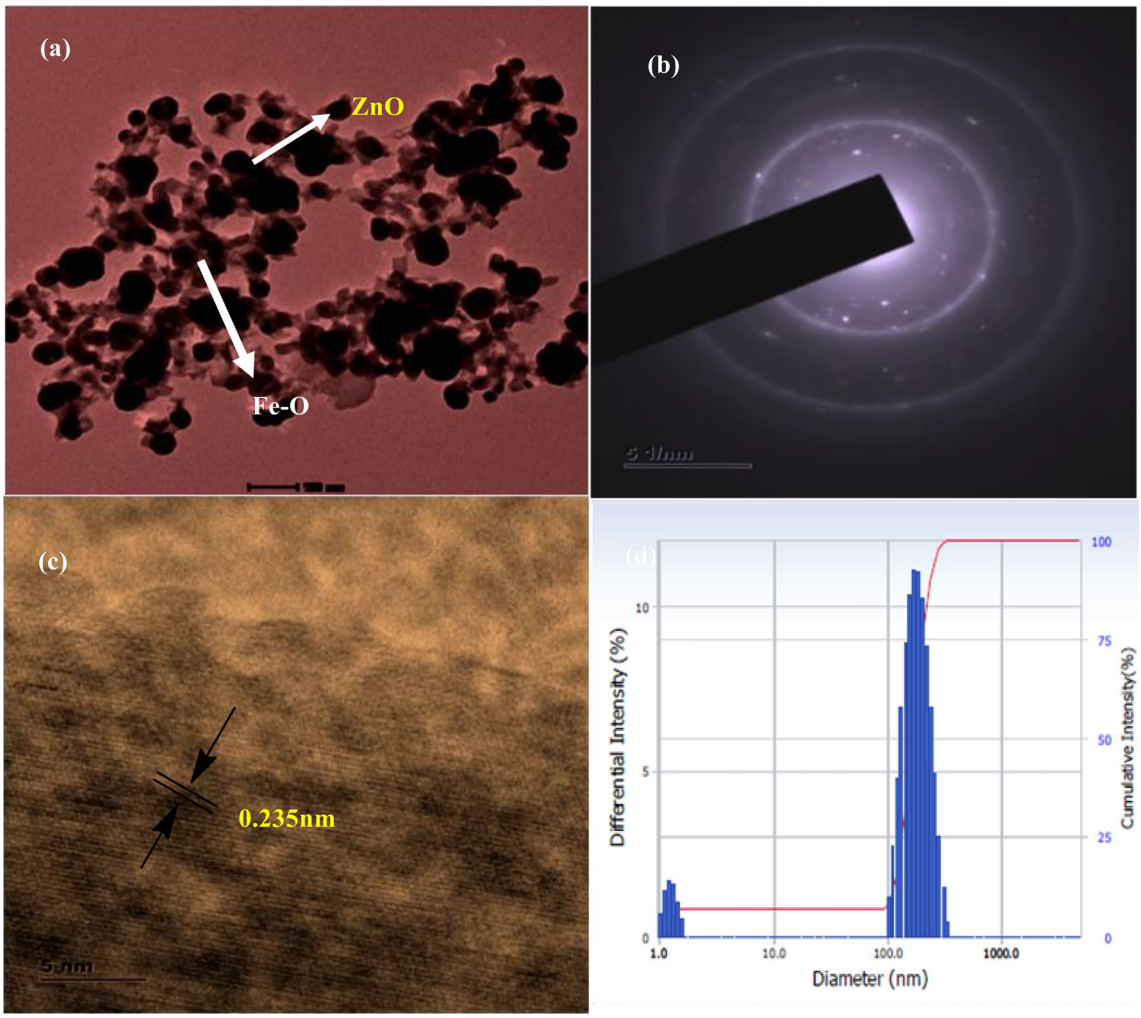


Fig. 5 **a** TEM profile of Fe_3O_4/ZnO, **b** SAED pattern analysis of Fe_3O_4/ZnO, **c** HR-TEM profile of Fe_3O_4/ZnO, **d** DLS analysis of Fe_3O_4/ZnO via greener route

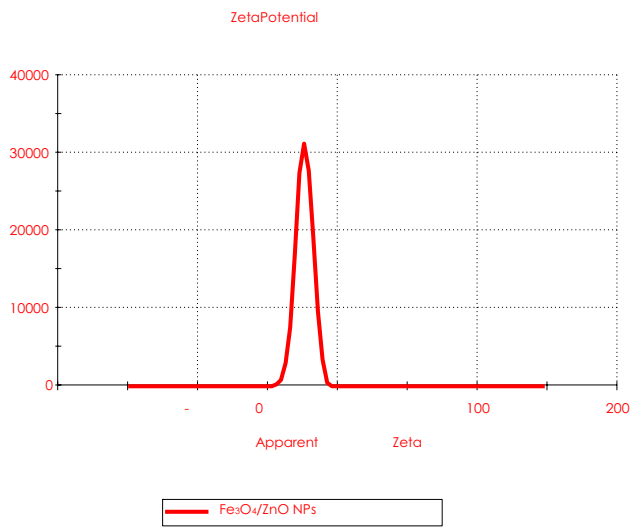


Fig. 6 Zeta potential analysis of Fe_3O_4/ZnO nanoparticles by greener way

Magnetic behavior analysis

According to the field-dependent magnetic properties graphs (Fig. 7a), the magnetization interaction of both Fe_3O_4 and Fe_3O_4/ZnO nanoparticles is pricey but nearly sequential at lower energies, and while at greater domains, the fragments are nearly connected with the applied magnetic field and the magnetization strategies saturation. The coercivity and remnant magnetization of Fe_3O_4 NPs were measured to be 15 Oe and 0.3 emu/g, respectively, whereas those Fe_3O_4/ZnO nanoparticles had been 17.5 Oe and 0.8 emu/g. The presence of fairly minimal coercivity and remnant magnetization indicates that these materials showed superparamagnetic actions at ambient temperature. Besides that, at 5 T, the maximum magnetic moment value of Fe_3O_4@ZnO nanoparticles (31.2 emu/g) was realized to be substantially lower than that of Fe_3O_4 NPs (35.8 emu/g). Magnetic moment has revealed that the ZnO shell in Fe_3O_4/ZnO NPs contributed

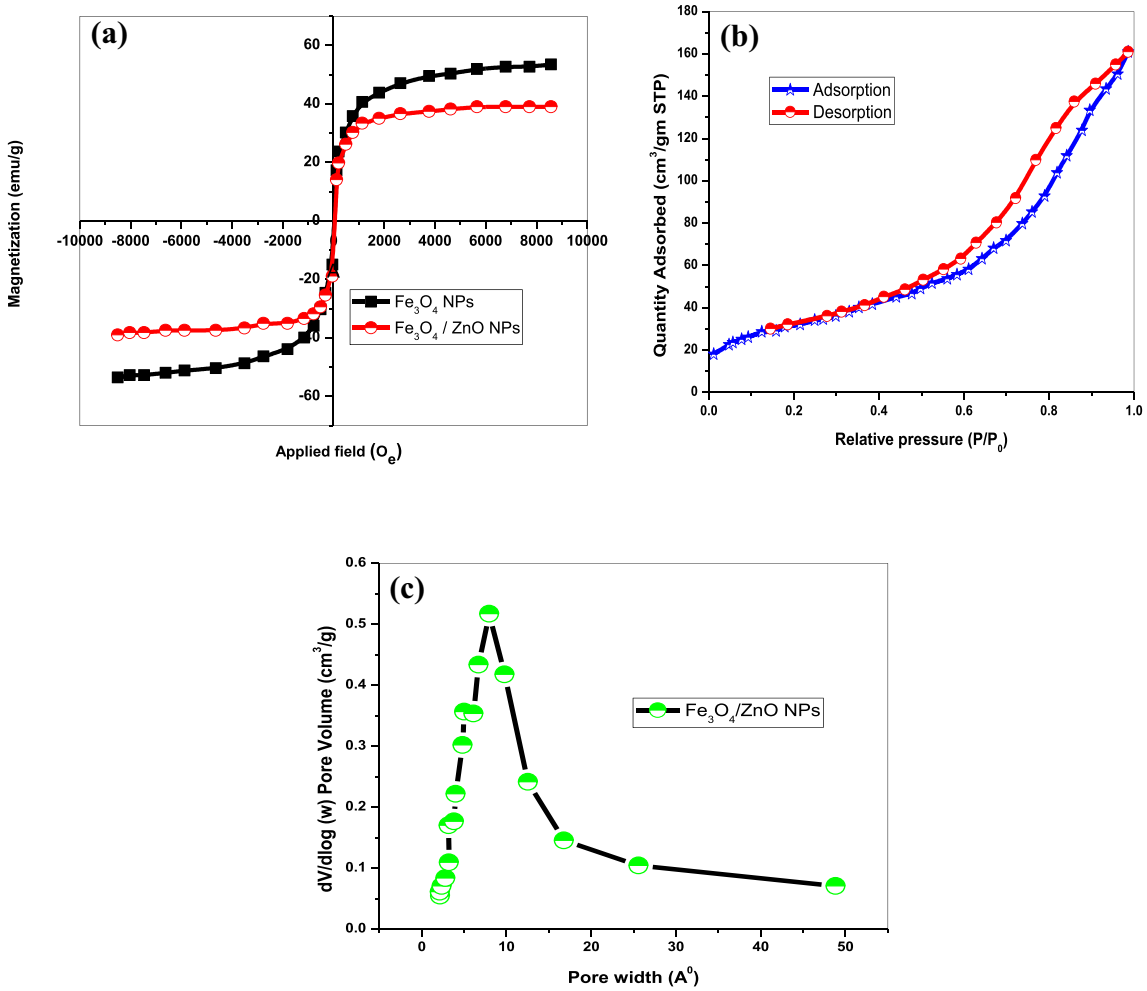


Fig. 7 **a** VSM spectra of Fe_3O_4 and Fe_3O_4/ZnO nanoparticles, **b** BET isotherm study, **c** pore width of synthesized Fe_3O_4/ZnO nanoparticles

significantly to a 12% lowering in the magnetic moment value of Fe_3O_4. As a consequence, the excellent magnetic field responsiveness of Fe_3O_4/ZnO is sustained. [29].

Variation impact of heavy metals

Impact of temperature

Effect of temperature is one of the most important parameters in the absorption process. Figure 8b represents the influence of temperature on the adsorption capacity of Fe_3O_4 @ ZnO nanoparticles in the range of 30–60 °C at room temperature. As it is shown in Fig. 8b, it is obvious that increasing temperature results in an increase of Pb(II), Cd(II), and Cr(IV) removal from aqueous solution. As depicted, adsorption was fast and equilibrium reached after 2 h. This rapid adsorption can be attributed to high dispersion of nanoparticles, high external surface area and lack of internal diffusion limitation [30, 31]. After the 10 min, there was little change in the absorption rate and it reflects that process would reach the equilibrium state. The optimum temperature for the adsorption using NCs was Fe_3O_4/ZnO achieved at 50 °C. As a result, to ensure complete equilibrium state, all of the experiments were performed for 60 °C.

Effect of adsorbent dosage

The effect of adsorbent dosage on the adsorption capacity and removal efficiency was investigated using various doses of nanoparticles. From Fig. 8a, removal efficiency of Pb(II), Cd(II), and Cr(IV) increases from 26.97 to 96.08% with an increase in the amount of adsorbent from 0.1 to 2 g L^{-1}. This is due to more availability of binding sites. On the other hand, adsorption capacity decreases from 269.7 to 48.04 mg g^{-1} with an increase in adsorbent dosage in the same range. The reason for this phenomenon is that existence ions were not enough for saturation of active sites with increasing adsorbent dosage. Actually adsorption capacity depends on metal-to-binding sites ratio.

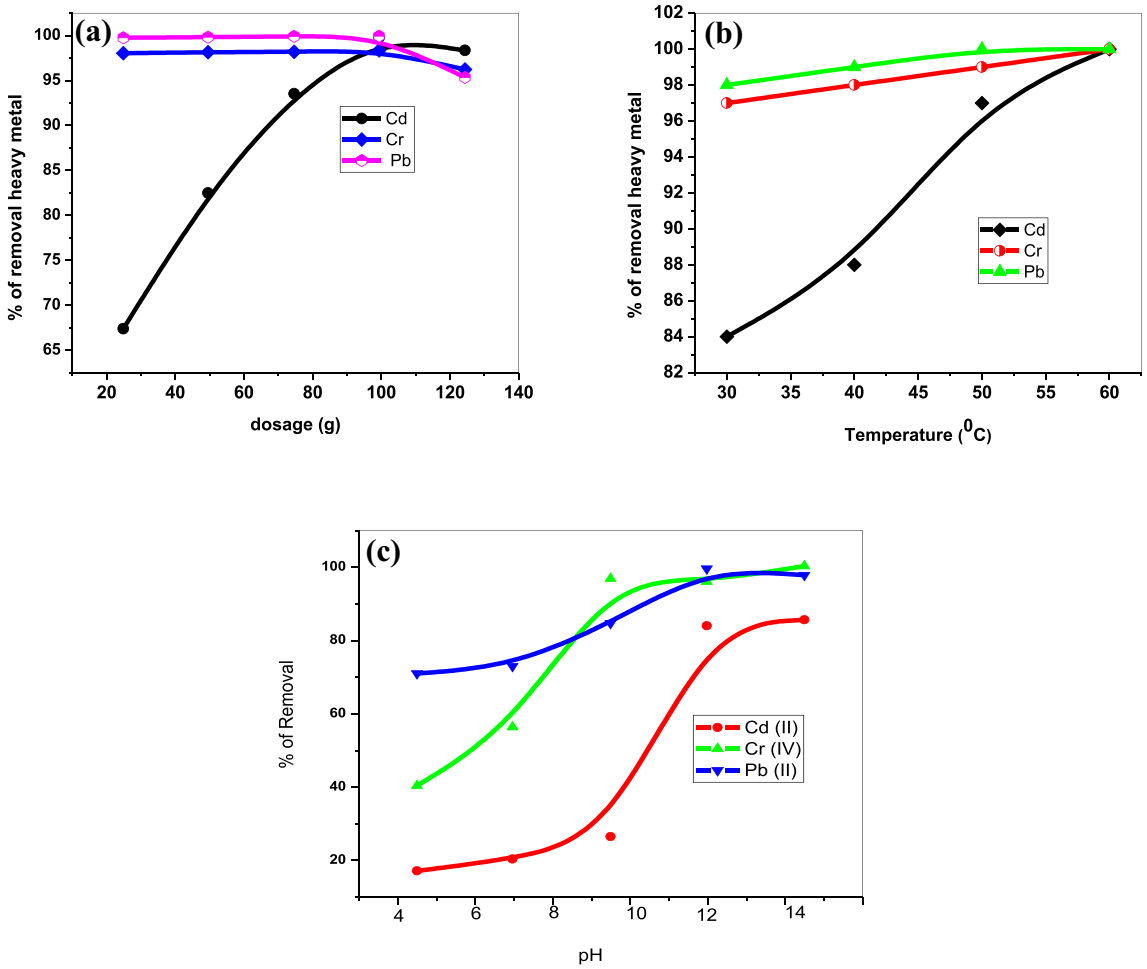


Fig. 8 **a** Effect of dosage dependent, **b** effect of temperature, **c** effect of pH

Effect of pH

The pH of the watery arrangement might be the main boundary in the adsorption cycle which influences metal particles and surface charge of adsorbent [32, 33]. Since at pH > 12 the Pb(II), Cd(II), and Cr(IV) particles begin to hasten, the examinations were done at pH 3–14 [34, 35]. As found in Fig. 8c, expanding pH brings about an expanding adsorption limit from 68.55 to 108.58 mg/g. The justification for this outcome is that higher pH leads to more deprotonation of adsorbent surface that expands negative charged locales, which is favor for electrostatic fascination between surface of adsorbent and Pb(II), Cd(II), and Cr(IV)particles, and consequently builds the adsorption limit (Fig. 9). However, lower pH leads to all the more decidedly charged destinations, which expands shock powers between adsorbent surface and Pb(II), Cd(II), and Cr(IV) particles that diminish the adsorption limit. Thus, pH 10–12 was considered for additional tests. Table 4 shows that the effect of Fe_3O_4/ZnO on commercial effluents was correlated in various studies [35–41].

Adsorption thermodynamic

The thermodynamic studies transforming in normal free energy change $G°$ 2 (J mol^{-1}), enthalpy $H°$ (J mol^{-1}), and entropy $S°$ (J mol^{-1} K^{-1}) were estimated using the three thermodynamic arithmetic [42, 43]

$$K_D = q_e/C_e \tag{8}$$

$$\Delta G^0 = -RT \ln K_D \tag{9}$$

$$\ln K_D = \Delta S^0/R - \Delta H^0/RT \tag{10}$$

The findings demonstrate that as the temperature is raised from 25 to 50 °C, the adsorption efficiency of nanoparticles decreased from Fe_3O_4/ZnO 109.1583–92.9709

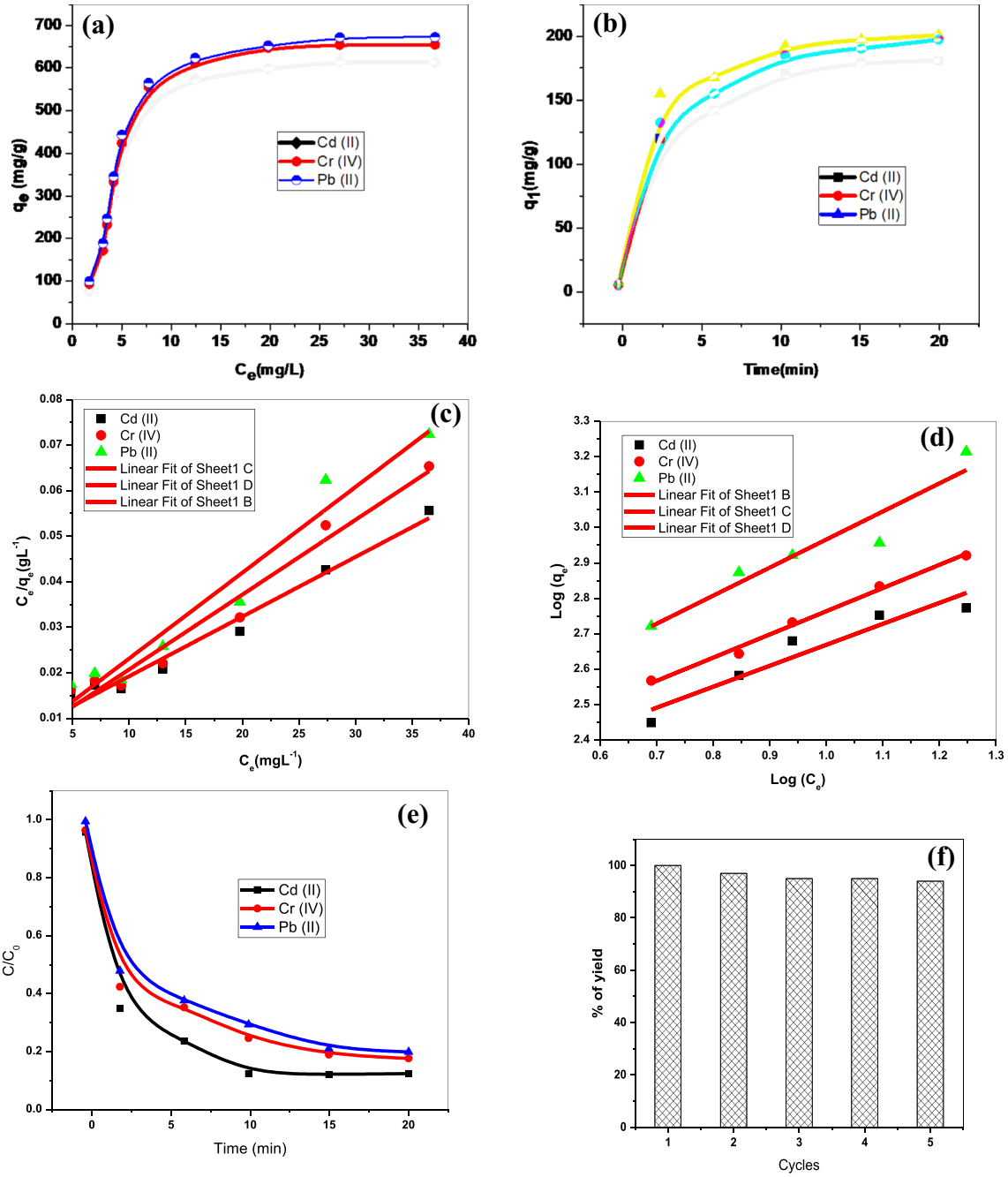


Fig. 9 **a** Experimental maximum Adsorption of isotherm of Cd(II), Cr(IV), Pb(II) on Fe_3O_4/ZnO, **b** experimental maximum adsorption of capability with time, **c** Langmuir isotherm model, **d** Freundich isotherm model, **e** kinetic plot, **f** reusability of Fe_3O_4/ZnO nanoparticles

(mg g^{-1}). This result suggests that the adsorption mechanism is thermodynamically favorable in exothermic reactions. The slope and intercept of versus can be used to correspond to values of $H°$ and $S°$. In addition, using Eq., the ln$G°$ value was K_D 1/T (10). Table 3 displays the determined thermodynamic properties. A negative $H°$ indicates that the adsorption of Cd(II), Cr(IV) and Pb(II) onto MNPs in nature is exothermic Fe_3O_4/ZnO. A negative value for S° denotes a reduction in the degree of freedom for adsorption species. Critical G° also proves the component's feasibility and intentional electrostatic interactions. Similar results have been obtained for the adsorption of Pb(II) by a nanopowder/alginate composite [44, 45].

Table 4 Various studies of adsorption capacity and other parameters for adsorption of anions by magnetic adsorbents

S.no	Adsorbents	Contact time	Optimal pH	Temperature °C	Concentration range	Adsorbent capacity	Pollutant	References
1	Fe_3O_4-coated glycine-doped polypyrrole magnetic nanocomposite	24 h	2	25–45	–	238 mg g^{-1} @ 25 °C	Cr(VI)	[35]
2	Magnetic hydroxyapatite	24 h	5 ± 0.1	25 ± 1	10–4–10–2 mol L^{-1}	1.964 mmol g^{-1} for Cd (II) 2.151 mmol g^{-1} for Zn (II)	Cd(II), Zn(II)	[36]
3	Magnetic alginate beads from sodium alginate	12 h	7	30	100–400 mg	50 mg g^{-1}	Pb(II)	[37]
4	Nanoscale zero valent iron particles	5 min	Neutral	–	100 µg mL^{-1}	100% removal for Pb(II), 100% removal for Cr (VI) 80% removal for Cd (II)	Pb(II), Cr(VI), Cd(II)	[38]
5	Polyethylenimine grafted magnetic adsorbent	10 min	6.5	Room temperature	100–600 mg L^{-1}	Ni (II)-49.6 mg g^{-1} Cu(II)-51.7 mg g^{-1} Cu(II)-157.8 mg g^{-1}	Ni(II), Cu(II), Cu(II)	[39]
6	Fe_3O_4 & silica-xanthan gum composite	240 min	6	20	10–100 mg L^{-1}	21.32 mg g^{-1}	Pb(II)	[40, 41]
7	Fe_3O_4/ZnO nanocomposites	2 h	7	60	100 mg L^{-1}	670.67 mg g^{-1} Pb(II), 99.81% Cr(VI) 99.76% Cd(II) 98.1%	Pb(II), Cr(VI), Cd(II)	Present study

Conclusion

The study conducted by on synthesis of Fe_3O_4/ZnO focuses on removing antibiotics from surface water bodies. Sequential bioreactor was used for the synthesis of nanocomposites and its photocatalytic performance was studied. Though SBR is a novel method used to synthesize nanocomposites it requires a sophisticated working system. Green synthesis of nanocomposite was used in the research which is cleaner, safer, and cost-effective to the environment. In this investigation, nanocomposites with a core–shell structure have been organized by using Fe_3O_4/ZnO nanocomposites presented two-stage approach and are used as an ideal alternative for lead, chromium, and cadmium metal ion revocation from aqueous medium. This sorbent was characterized using various tools like UV–Vis, XRD, EDS, FTIR, VSM, FESEM, TEM, and BET assessment. Adsorbent was rapid, and stability was reached in around 2 h. The adsorbent method can be easily outlined by a pseudo-second-order kinetic template. The Langmuir isotherm model may better fit the equilibrium data than the Freundlich isotherm prototypes. Even so, the maximum adsorption capability was 670.67 mg g^{-1}. $G°$, $H°$, and S values were determined. Negative numbers of $G°$ and $H°$ indicate an attainable and exothermic adsorption mechanism, respectively. Such findings suggest that Fe_3O_4/ZnO nanocomposites might be used as a completely new Fe_3O_4/ZnO adsorbent for the elimination of Pb(II), Cr(IV), and Cd(II) ions from commercial effluent. Nanocomposite of Fe_3O_4/ZnO was able to remove antibiotics at optimized parameters of pH 7, H_2O_2 (100 mg L^{-1}), and catalyst concentration of (100 mg L^{-1}). In this study, the optimized parameters the absorption increased from pH 10–12, metal-to-binding sites ratio, equilibrium at 60 °C the nanocomposite were able to effectively remove heavy metals from industrial effluents. Thus, greener synthesis and optimized Fe_3O_4/ZnO can remove effluents for numerous cycles.

Acknowledgements This research did not receive any specific grant from funding in the public, commercial or not for profit sectors.

Declarations

Conflict of interest The authors have declared that they have no conflict interest.

References

1. B. Dhir, Potential of biological materials for removing heavy metals from wastewater. Environ. Sci. Pollut. Res. **21**, 1614–1627 (2014)
2. S.H. Abdel-Halim, A.M. Shehata, M.F. El-Shahat, Removal of lead ions from industrial waste water by different types of natural materials. Water Res. **37**, 1678–1683 (2003)
3. F. Barbosa Jr., Toxicology of metals and metalloids: promising issues for future studies in environmental health and toxicology. J. Toxicol. Environ. Health Part A **80**(3), 137–144 (2017)
4. J. Acharya, U. Kumar, B. Meikap, Thermodynamic characterization of adsorption of lead (II) ions on activated carbon developed from tamarind wood from aqueous solution. S. Afr. J. Chem. Eng. **18**, 70–76 (2013)
5. B. Singha, S.K. Das, Removal of Pb(II) ions from aqueous solution and industrial effluent using natural biosorbents. Environ. Sci. Pollut. Res. **19**, 2212–2226 (2012)
6. J. Hu, D. Zhao, X. Wang, Removal of Pb(II) and Cu(II) from aqueous solution using multiwalled carbon nanotubes/iron oxide magnetic composites. Water Sci. Technol. **63**, 917–923 (2011)
7. L. Dong, Z. Zhu, Y. Qiu, J. Zhao, Removal of lead from aqueous solution by hydroxyapatite/magnetite composite adsorbent. Chem. Eng. J. **165**, 827–834 (2010)
8. İ Kara, D. Yilmazer, S.T. Akar, Metakaolin based geopolymer as an effective adsorbent for adsorption of zinc(II) and nickel(II) ions from aqueous solutions. Appl Clay Sci. **139**, 54–63 (2017)
9. R. Qiu, F. Cheng, H. Huang, Removal of Cd from aqueous solution using hydrothermally modified circulating fluidized bed fly ash resulting from coal gangue power plant. J. Clean Prod. **172**, 1918–1927 (2018)
10. M.F. Horst, M. Alvarez, V.L. Lassalle, Removal of heavy metals from wastewater using magnetic nanocomposites: analysis of the experimental conditions. Sep. Sci. Technol. **51**, 550–563 (2016)
11. M. Hua et al., Heavy metal removal from water/wastewater by nanosized metal oxides: a review. J. Hazard Mater. **211**(15), 317–331 (2012)
12. C.L. Warner, W. Chouyyok, K.E. Mackie, D. Neiner, L.V. Saraf, T.C. Droubay, M.G. Warner, R.S. Addleman, Manganese doping of magnetic iron oxide nanoparticles: tailoring surface reactivity for a regenerable heavy metal sorbent. Langmuir **28**, 3931–3937 (2012)
13. J. Yan, E. Khoo, A. Sumboja, P.S. Lee, Facile coating of manganese oxide on tin oxide nanowires with high-performance capacitive behavior. ACS Nano **4**(7), 4247–4255 (2010)
14. D. Habibi, S. Kaamyabi, H. Hazarkhani, Chin. J. Catal. **36**, 362 (2015)
15. S.P. Rajendran, K. Sengodan, Hindawi J. Nanosci. **2017**, 1 (2017)
16. I. Langmuir, The constitution and fundamental properties of solids and liquids. Part I. Solids. J. Am. Chem. Soc. **38**, 2221–2295 (1916)
17. O.S. Nuri, M. Irannajad, A. Mehdilo, Reagent adsorption on modified mineral surfaces: isotherm, kinetic and thermodynamic aspects. J. Mol. Liq. **291**, 111311 (2019)
18. E. Li, H. Liang, Z. Du, D. Li, F. Cheng, Adsorption process of octadecylamine hydrochloride on KCl crystal surface in various salt saturated solutions: kinetics, isotherm model and thermodynamics properties. J. Mol. Liq. **221**, 949–953 (2016)
19. X. Fuku, A. Diallo, M. Maaza, Nanoscaled electrocatalytic optically modulated ZnO nanoparticles through green process of *Punica granatum* L. and their antibacterial activities. J. Electrochem. Int. (2016). https://doi.org/10.1155/2016/4682967
20. X. Fuku, K. Kaviyarasu, N. Matinise, M. Maaza, Punicalagin green functionalized Cu/Cu_2O/ZnO/CuO nanocomposite for potential electrochemical transducer and catalyst. Nanoscale Res. Lett. **11**(1), 386 (2016)
21. N. Matinise, X.G. Fuku, K. Kaviyarasu et al., ZnO nanoparticles via *Moringa oleifera* green synthesis: physical properties & mechanism of formation. Appl. Surf. Sci. **406**, 339–347 (2017)
22. J. Gupta, P.A. Hassan, K.C. Barick, Core-shell Fe_3O_4@ZnO nanoparticles for magnetic hyperthermia and bio-imaging applications. AIP Adv. **11**, 025207 (2021)
23. N.K. Sethy, Z. Arif, P.K. Mishra, P. Kumar, Green synthesis of TiO_2 nanoparticles from *Syzygium cumini* extract for photo-catalytic removal of lead (Pb) in explosive industrial wastewater. Green Process Synth. **9**, 171–181 (2020)
24. K.S. Saranya, V.V.T. Padil, C. Senan, R. Pilankatta, K. Saranya, B. George et al., Green synthesis of high temperature stable anatase titanium dioxide nanoparticles using gum Kondagogu: characterization and solar driven photocatalytic degradation of organic dye. Nanomater. Basel **8**, 1002–1021 (2018)
25. M.T. Thein, S.-Y. Pung, A. Aziz, M. Itoh, Stacked ZnO nanorods synthesized by solution precipitation method and their photocatalytic activity study. J. Sol. Gel Sci. Technol. **74**, 260–271 (2015)
26. X. Wang, W. Cai, Y. Lin, G. Wang, C. Liang, Mass production of micro/nanostructured porous ZnO plates and their strong structurally enhanced and selective adsorption performance for environmental remediation. J. Mater. Chem. **20**, 8582–8590 (2010)
27. J. Xu, X. Han, H. Liu, Y. Hu, Synthesis and optical properties of silver nanoparticles stabilized by gemini surfactant. Colloid Surf A. **273**, 179–183 (2006)
28. K. Kucharczyk, J.D. Rybka, M. Hilgendorff et al., Composite spheres made of bioengineered spider silk and iron oxide nanoparticles for theranostics applications. PLoS ONE **14**, e0219790 (2019)
29. N.N. Nassar, Kinetics, equilibrium and thermodynamic studies on the adsorptive removal of nickel, cadmium and cobalt from wastewater by superparamagnetic iron oxide nanoadsorbents. Can. J. Chem. Eng. **90**, 1231–1238 (2012). https://doi.org/10.1002/cjce.20613
30. H. Shayesteh, A. Rahbar-kelishami, R. Norouzbeigi, Evaluation of natural and cationic surfactant modified pumice for congo red removal in batch mode: kinetic, equilibrium, and thermodynamic studies. J. Mol. Liq. **221**, 1–11 (2016). https://doi.org/10.1016/j.molliq.2016.05.053
31. R.D.C. Soltani, G.S. Khorramabadi, A.R. Khataee, S. Jorfi, Silica nanopowders/alginate composite for adsorption of lead (II) ions in aqueous solutions. J. Taiwan Inst. Chem. Eng. **45**, 973–980 (2014). https://doi.org/10.1016/j.jtice.2013.09.014
32. Z. Shu, S. Wang, Synthesis and characterization of magnetic nanosized/composite particles. J. Nanomater. **2009**, 1–5 (2009). https://doi.org/10.1155/2009/340217
33. N.N. Nassar, Rapid removal and recovery of Pb(II) from wastewater by magnetic nanoadsorbents. J. Hazard. Mater. **184**, 538–546 (2010). https://doi.org/10.1016/j.jhazmat.2010.08.069
34. D. Mehta, S. Mazumdar, S.K. Singh, Magnetic adsorbents for the treatment of water/wastewater—a review. J. Water Process Eng. **7**, 244–265 (2015). https://doi.org/10.1016/j.jwpe.2015.07.001
35. J. Chen, F. He, H. Zhang, X. Zhang, G. Zhang, G. Yuan, Novel core-shell structured Mn–Fe/MnO_2 magnetic nanoparticles for enhanced Pb(II) removal from aqueous solution. Ind. Eng. Chem. Res. (2014). https://doi.org/10.1021/ie502967a

36. N. Ballav, H. Choi, S. Mishra, A. Maity, Synthesis, characterization of Fe_3O_4@glycine doped polypyrrole magnetic nanocomposites and their potential performance to remove toxic Cr(VI). J. Ind. Eng. Chem. **20**, 4085–4093 (2014)
37. Y. Feng, J.-L. Gong, G.-M. Zeng, Q.-Y. Niu, H.-Y. Zhang, C.-G. Niu et al., Adsorption of Cd (II) and Zn (II) from aqueous solutions using magnetic hydroxyapatite nanoparticles as adsorbents. Chem. Eng. J. **162**, 487–494 (2010)
38. A. Idris, N.S. Ismail, N. Hassan, E. Misran, A.-F. Ngomsik, Synthesis of magnetic alginate beads based on maghemite nanoparticles for Pb(II) removal in aqueous solution. J. Ind. Eng. Chem. **18**, 1582–1589 (2012)
39. Z.Y. Lin, Y.X. Zhang, Y.L. Chen, H. Qian, Extraction and recycling utilization of metal ions (Cu^{2+}, Co^{2+} and Ni^{2+}) with magnetic polymer beads. Chem. Eng. J. **200**, 104–112 (2012)
40. Y. Pang, G. Zeng, L. Tang, Y. Zhang, Y. Liu, X. Lei et al., PEI-grafted magnetic porous powder for highly effective adsorption of heavy metal ions. Desalination **281**, 278–284 (2011)
41. X. Peng, F. Xu, W. Zhang, J. Wang, C. Zeng, M. Niu et al., Magnetic Fe_3O_4@silica–xanthan gum composites for aqueous removal and recovery of Pb^{2+}. Colloids Surf. A Physicochem. Eng. Aspects **443**(27), 36 (2014)
42. A.Z.M. Badruddoza, S.H. Tay, P.Y. Tan, K. Hidajat, M.S. Uddin, Carboxymethyl-β-cyclodextrin conjugated magnetic nanoparticles as nano adsorbents for removal of copper ions: synthesis and adsorption studies. J. Hazard. Mater. **185**, 1177–1186 (2011)
43. M. Demirkurt et al., Electrospun polystyrene fibers knitted around imprinted acrylate microspheres as sorbent for Paraben derivatives. Anal. Chim. Acta **1014**, 1–9 (2018). https://doi.org/10.1016/j.aca.2018.02.016
44. I. Márquez-Sillero et al., Determination of parabens in cosmetic products using multi-walled carbon nanotubes as solid phase extraction sorbent and corona-charged aerosol detection system. J. Chromatogr. A **1217**(1), 1–6 (2010)
45. L. Fernández et al., Insight into antibiotics removal: Exploring the photocatalytic performance of a Fe_3O_4/ZnO nanocomposite in a novel magnetic sequential batch reactor. J. Environ. Manag. **237**, 595–608 (2019). https://doi.org/10.1016/j.jenvman.2019.02.089

Springer Nature or its licensor (e.g. a society or other partner) holds exclusive rights to this article under a publishing agreement with the author(s) or other rightsholder(s); author self-archiving of the accepted manuscript version of this article is solely governed by the terms of such publishing agreement and applicable law.